OBSERVATIONAL STUDIES AND INTERPRETATION OF THE MOUNTAIN PRESSURE DRAG DURING ALPEX

H.C. Davies
Atmospheric Physics, ETH
Zürich, Switzerland

Summary: A brief overview is given of the various pressure drag studies undertaken for the European Alps with data gathered during the two-month special observational period of the ALPEX project. Also some comments are made on the nature of various signatures associated with the temporal variations of the pressure drag during this period.
The study is developed within a framework composed of a consideration of the momentum budget for a limited portion of the atmosphere together with a summary of theoretical studies of flow processes that can sustain a pressure force on mesoscale orography.

1. INTRODUCTION

A ubiquitious feature of the atmosphere is the existence of horizontal pressure gradients in mountainous regions. The accompanying pressure difference experienced at a given level across a mountain constitues a stress acting at the earth-atmosphere interface. These pressure-induced interfacial stresses influence the temporal variations of the various components of the solid earth's angular momentum, and also the atmosphere's flow dynamics. In the geophysical context the pressure force on a given terrain feature is merely the local contribution to the net global surface pressure torque. On the other hand, from an atmospheric fluid flow standpoint, that local pressure force is itself inextricably linked with the "local" flow dynamics, and the precise form of the linkage depends sensitively upon both the horizontal spatial scale and the height of the orography.
This study is principally concerned with the pressure force exerted on the European Alps, a major mesoscale mountain range. In the next section brief consideration is given to the momentum budget for a limited portion of the atmosphere. This provides a framework for some general comments on both the conventional nomenclature adopted in studies of the orographic pressure force and on the mesoscale flow phenomena that can offset that force.

Section 3 is a summary of the studies undertaken to estimate the synoptic/sub-synoptic scale pressure force acting on the Alps during the two-month special observational period (SOP) of the international ALPEX project. The subsequent section is devoted to an interpretation of these results in relation to the prevailing flow patterns.

2. PRELIMINARY CONSIDERATIONS

2.1 Momentum budget for a limited-domain

For illustrative purposes consider the flow of an incompressible Boussinesq fluid over an isolated orographic feature mounted on an f-plane. Then for a fixed volume $\mathcal{V}$ (see Fig. 1) bounded below by a portion of the earth's surface S_G and elsewhere by the purely geometric surface (S_L, S_T), the time rate of change of the net x - directed momentum M ($= \rho_0 u$) is given by,

$$\frac{\partial}{\partial t}\iiint_{\mathcal{V}} M \, d\mathcal{V}$$

$$= -\iint_{S_L+S_T} M(\underset{\sim}{v}\cdot\underset{\sim}{n})\,ds + f\iiint_{\mathcal{V}}(\rho_0 v)\,d\mathcal{V} - \iint_{S_G+S_L+S_T}\{p(\underset{\sim}{n}\cdot\underset{\sim}{i}) - \mu(\nabla u\cdot\underset{\sim}{n})\}\,ds \qquad (2.1)$$

The terms on the right hand side of this equation represent respectively

- the net momentum flux across the open boundaries (this comprises the sum of the advective flux associated with mean flow, the coherent wave flux, and the turbulent flux),
- the v-component of the Coriolis body force acting on this limited volume of fluid, and
- the net pressure and viscous stress effects acting over the entire surface.

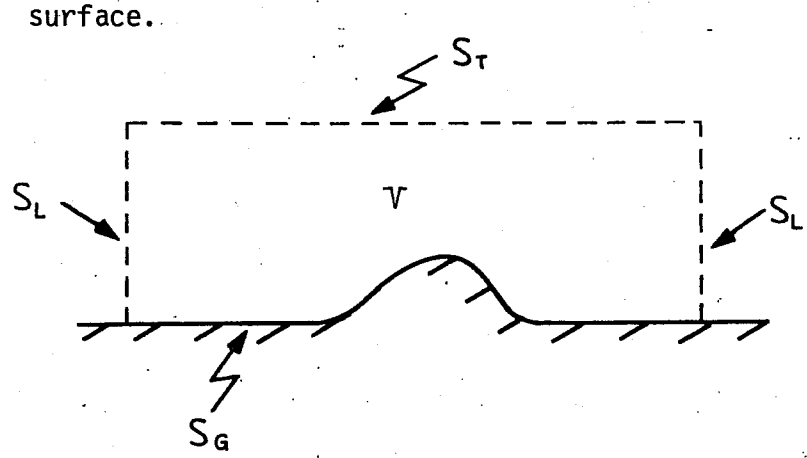

Fig. 1

Schematic of the limited region considered for the momentum budget. The ground surface is given by S_G, whilst S_L and S_T are open, purely geometric surfaces immersed in the fluid.

It is the "S_G" - contribution to the last integral that defines the x - component of the net surface stress within the limited domain. The form of the expression for the pressure contribution to this ground stress is evident from the following decomposition,

$$\iint_{S_G + S_L + S_T} p(\underset{\sim}{n} \cdot \underset{\sim}{i})\, ds = -\iint_{S_G} (\Delta p)\, dy\, dz + \iint_{S_L} (\mathcal{D}p)\, dy\, dz$$

$$= I_G + I_L \qquad (2.2)$$

where $\Delta p = \Delta p(y,z)$ is the east-west horizontal pressure difference across the orographic feature at a given height, and similarly (Dp) is the horizontal pressure difference across the entire limited domain. It is self-evident, but nevertheless instructive, to note that the dynamics of a flow that realizes a pressure related surface stress might be linked to one of, or a combination of, the other budget terms. To emphasize this fact we list below some special cases of momentum balance:

(i) A steady state flow of an inviscid fluid that is aligned in the y-direction would correspond to a balance between the surface pressure force (I_G) and the Coriolis body-force.

(ii) A stationary flow field within the entire volume $\mathcal{V}$ accompanied by a non-zero I_G contribution must be offset by a lateral boundary pressure force (I_L). In this case the orographic pressure force either indirectly sustains flow in the fluid exterior to $\mathcal{V}$, or is compensated by an orographic effect elsewhere. The trapping of a low-level layer of cold air between two mountain ridges or the up- or down-stream propagation of a "bore-like" phenomenon could yield such an effect.

(iii) In the inviscid (μ=0), non-rotating (f=0) limit, a steady state flow that is identical at the up- and down-stream boundaries could nevertheless sustain a non-zero I_G by the import of wave momentum across the upper boundary.

2.2 Nomenclature

The sum of the pressure and viscous contributions to the surface stress is often referred to (somewhat loosely) as the net drag. There are several traditional sub-divisions of this net drag. For example engineering terminology ascribes the expressions "Drag" and "Lift" for the components that are respectively in the direction of, and normal to the incident flow. However it is not always feasible to attempt this distinction in mesoscale atmospheric applications. In this realm the incident flow can (and frequently does) exhibit a significant turning with altitude below the mountain crest height.

Moreover transience and the possibility of appreciable and spatially extensive upstream influence upon the low-level air are other complicating factors. A more fundamental distinction would seek to isolate the contribution to the net stress that is associated with "flow-resisting" dissipative processes (- a point emphasised in the seminar series by P. Mason).
A second sub-division into "aerodynamic" and "pressure" components arises as follows. Turbulence in the planetary boundary layer plays only an indirect role in establishing the actual surface drag; it merely modifies the near surface pressure and velocity fields. However an expectation, for example, of an almost constant stress layer atop of the viscous sub-layer would link the Reynolds stresses of the turbulent flow directly with the surface drag. Thus in practice it has been customary to describe the net-effect of almost homogeneous micro-scale surface elements in terms of the near-surface turbulent Reynolds stresses and to identify this contribution as the aerodynamic drag. The remaining component, by default and/or by analogy with the original two components of the net stress in Eq. (2.1), is referred to as the pressure drag.
A further conceptually attractive sub-division of the pressure drag is to split it into the two components: form drag (D_f) and wave drag (D_w). A distinction between these two components can be made once it is recognised that a dissipation-related pressure drag is accompanied by an energy transport away from the terrain, and that this transport can be effected by different processes. A natural extension of the customary terminology would be to take form and wave drag to signify essentially that the primary mode of the

transport is accomplished respectively by

- advection of turbulent eddy energy away within the mean flow,
- transmission of energy through the mean flow in a coherent wave-like, or at least a wave-related, form.

The first process takes place predominantly in the planetary boundary layer and most of the eddy energy is probably dissipated within a distance typically ~ 10 L downstream (where L is a scale width of the obstacle). On the other hand in the second process the expectation is that the energy propagates away with the group velocity, and the ray path and rate of dissipation of the wave packet is dependent upon the transmissivity properties of the atmospheric medium. An important limitation of this sub-division is that the processes can coexist and an interaction between them can not be ruled out. This implies that it might be inappropriate to attempt to establish their relative importance in given atmospheric flow situation.

2.3 Mesoscale phenomena and pressure drag

A key dynamical feature associated with flow incident upon mesoscale orography is the possibility of a wave-drag resulting from the vertical propagation of buoyancy-wave energy away from the obstacle and a concomitant transfer of horizontal momentum in the opposite direction. In the limit of linear theory it can be shown that, for an uniform flow field (U) with a constant Brunt-Vaisala frequency (N), upward energy propagation is possible if

$$\mathcal{S} < \mathcal{I} < R_o$$

where $\mathcal{S} \sim U/NL$, $R_0 \sim U/fL$, and L is a measure of the horizontal length scale of the orography. The wave drag per unit length is $\sim\{\rho_o UNh^2/L\}$ in the middle of this $(\mathcal{S}-R_0)$ spatial-window and it reduces to zero at the fringes. The momentum balance in this case corresponds intimately with the special case (iii) discussed in section 2.1.

Theoretical studies undertaken at the lower end of this window (i.e. in the $R_0 \to \infty$ limit) and with uniform upstream conditions suggest that non-linear effects, expressed in terms of an inverse Froude number, $\mathcal{F} = Nh/U$, can substantially modify the flow pattern and the accompanying drag values. (Here h refers to the mountain height.) Changes in the response occur as $\mathcal{F}$ increases.

First there is a moderate increase in the pressure drag until the flow attains a wave-overturning amplitude. This occurs for example at $\mathcal{F} = 0.85$ for a bell-shaped obstacle (Lilly and Klemp, 1979). Thereafter the numerical model results of Peltier and Clark (1979) reveal a factor of ~ 4 enhancement of the drag. This enhancement is accompanied by a downstream energy transport as the wave activity appears to be substantially confined to a "resonant cavity" between the wave-overturning level and the ground. In such a flow the pressure drag on the orography sustains momentum changes downstream and this configuration has some kinship with the special case (ii) considered in section 2.1.

The foregoing studies emphasised the non-linear modification of the drag that can occur for uniform upstream conditions. However vertical variations in the N and U values of the incident airstream can also alter the transmissivity of the atmosphere to buoyancy waves, and this in turn can modify the pressure drag. The linear theory study of Klemp and Lilly (1975) and the extension to the non-linear regime using a numerical model (Durran, 1986) yield a drag change by a factor of $\sim$ (1/3 - 3) for these effects. The precise value depends sensitively on the form of the incident flow's vertical structure. Several other factors can strongly influence the nature of the wave response and the resulting pressure drag in this central portion of the $(\mathcal{S}, R_0)$ window. These include the orographic shape (Lilly and Klemp, 1979), the near-exponential decrease of the mean density that induces an increase of the amplitude as a wave packet propagates vertically, the existence of critical layers and/or small Richardson number layers in the free atmosphere (Bretherton, 1969), and the influence of cloud diabatic effects (e.g. Durran and Klemp, 1985; Jusem and Barcilon, 1985; Davies and Schär, 1986). Another significant factor is the juxtaposition of orographic ridges (Bell and Thompson, 1980).

The relationship of these studies to Alpine flow is brought out on noting that assuming a half-width of $\lesssim$ 100 km for the north-south extend of the Alps and a height of $\sim$ 2.5 km renders

$$\mathcal{S} \sim 10^{-4} \; ; \quad R_0 \gtrsim 1 \; ; \quad \mathcal{F} \sim 2.5 \, ,$$

for typical atmospheric values of N and U. Thus in a northerly flow situation the latitudinal envelope of the Alps constitutes a barrier that is at the upper end of the $(\mathcal{S}, R_0)$ window for vertical propagation. Also these

values for $\mathcal{F}$ and R_0 suggest the possible existence of non-linear effects akin to these associated with upstream blocking, a downstream resonant cavity and flow transition effects. However for the Alps these effects would probably be subject to strong rotational modification and also influenced by the finite length of the ridge.

Also the scale of Alpine topography is intermediate between two flow extremes both of which entail the formation of a distinctive columnar flow structure. These two categories correspond to the geostrophic unstratified limit ($R_0 \lesssim 1$, $\mathcal{F} \ll 1$) with a Taylor column above a mountain and a pressure force composed of a pure lift, and the non-rotating strongly stratified limit ($R_0^{-1} = 0, \mathcal{F} \gg 1$) with an upstream low-level layer of stationary fluid ahead of an infinite ridge.

Some studies have been undertaken that border upon this intermediate niche in parameter space associated with Alpine scale flow. Mason (1977) performed a laboratory examination of the drag and lift effects on a sphere moving through a rotating stratified fluid. Pierrehumbert (1985) and Davies and Horn (1987) examined theoretically the steady state orographic response in the semi-geostrophic, finite-amplitude limit of ($R_0 \lesssim 1, \mathcal{F} \sim 1$). The results of these latter studies suggest that, for the elongated ridge configuration, major flow departure from the geostrophic pattern of accelerated flow over the crest must occur for $\{R_0 \mathcal{F}/\mathcal{A}\} \gtrsim 1$, where $\mathcal{A}$ is a measure of the "smoothness" of the orography (with, for example, $\mathcal{A} \to 0$ for a "Chapeau"-type profile). This flow departure is most probably associated with non-linearly forced buoyancy waves and/or three-dimensional effects.

One of the few direct studies of the ($R_0 \gtrsim 1, \mathcal{F} \gtrsim 1$) intermediate portion of parameter space is that undertaken by Pierrehumbert and Wyman (1985). Their numerical model results indicate that, in the infinite ridge case for $F \gtrsim (1 - 2)$, the attainment of a wave-overturning amplitude heralds the onset of substantial upstream blocking of the low-level air. In momentum budget terms the results are consistent with the pressure drag being accompanied predominantly in a $Ro \gg 1$ regime by deacceleration to rest of a portion of fluid upstream, and by a flow turning to establish a Coriolis body force effect for a $R_0 \lesssim 1$ regime.

The establishment upstream of a blocked and/or strongly deflected layer of low-level air allows a lee-side downslope flow of an elevated air layer with a concomitant lee warning. The resulting pressure drag could be offset by flow transience, and by up- and down-stream velocity changes.

3. SUMMARY OF ALPEX PRESSURE DRAG STUDIES

Several pressure-drag studies (Hafner and Smith, 1985; Davies and Phillips, 1985; Hafner, 1985; Carissimo and Pierrehumbert, 1986) have been undertaken with observational data gathered during the two-month special observational period (March-April, 1982) of the ALPEX project. Hereafter these four studies will be referred to respectively as HS, DP, H and CP.

In DP and H estimates were derived for the meridional component of the pressure drag acting on a central Alpine section. The studies used the data from the special array of microbarograph aligned along the St. Gotthard section of the Alps (see Fig. 2). This section provides one of the simplest orographic profiles for a north-south transect of the Alps, and the barographs were disposed from Stuttgart in the north down to Acqui in the Po-valley in the south.

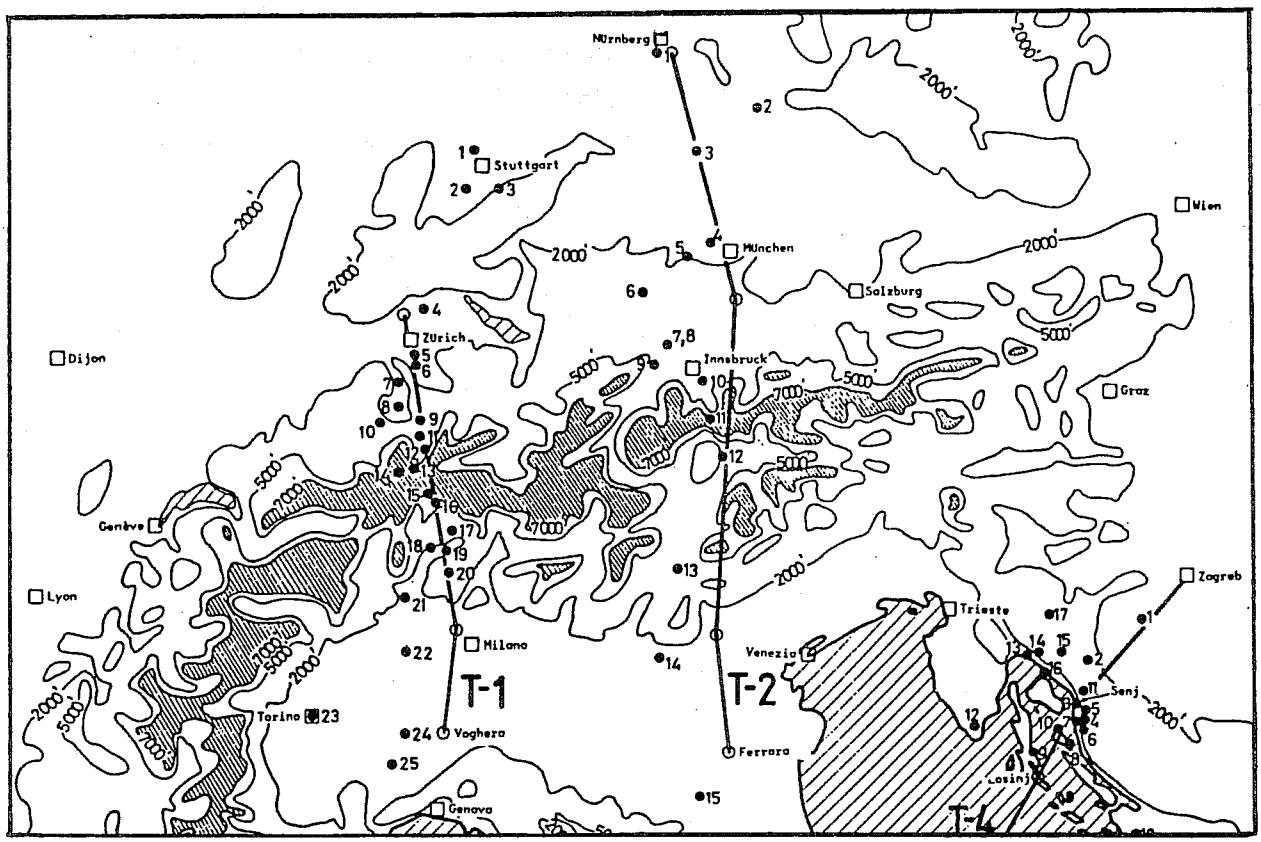

Fig. 2 A depiction of the Alpine region showing the location of the three microbaragraph arrays during ALPEX . The St. Gotthard array is the section denoted by T-1.

The station arrangement in the St. Gotthard section provided a spatial separation of $\sim$ 10 km in the inner-Alpine region, and the temporal resolution for almost all the stations was 10 minutes. To determine the drag in these studies it was necessary to evaluate the one dimensional form of the integral I_G of (2.2). This involved constructing a mathematical representation of the orography. The estimates of DP were derived for the drag acting on the 100 km inner-Alpine portion of this section and a smooth orographic profile was adopted on the premise that in this region the St. Gotthard constitutes an almost single ridge transect of the Alps. On the other hand H provides estimates of the drag for a 300 km strip from Stuttgart to near Lugano that includes both the Black Forest and the Gotthard section. In his study the pseudo-orographic profile is composed of a sequence of triangular features. The base of each feature correspond to the location of two neighbouring microbarographs and the height is a measure of the laterally averaged orography of that particular "inner-station"region.

A semi-schematic representation of the time trace of the drag obtained in the two studies for the March 1-12 period of ALPEX is shown in Figs. (3a,b). The (Nm^{-1}) scale on the right of both figures refers to the drag (say D/ℓ) expressed as a measure of the amplitude per unit of lateral length perpendicular to the Gotthard section. The Pascal scale on the left refers to a drag per unit area, say $(D/\Delta) = (D/\ell) \div L$. For Fig. 3a the "divisor-length" L has been set to 100 km, the length of the inner Alpine region considered in DP. However for interpretative purposes the divisor for the H study (Fig. 3b) has been set to half the length of the section used in the drag evaluation. The rationale is that it is indicated in H that a substantial percentage of the drag ($\sim$ 80%) is associated with the inner-Alpine region. A comparison of the two time traces (see Figs. 3a,b) reveals excellent phase agreement and, bearing in mind the rescaling of the (D/Δ) measurements, a reasonable accord of the amplitude response. The confinement of the horizontal pressure variations, and hence the drag to the meso $\alpha - \beta$ scale of the inner Alpine region is strikingly apparent in Fig. 4 which shows the time-trace of the horizontal pressure gradient to the north of, to the south of, and within the inner Alpine region, for the second half of March.

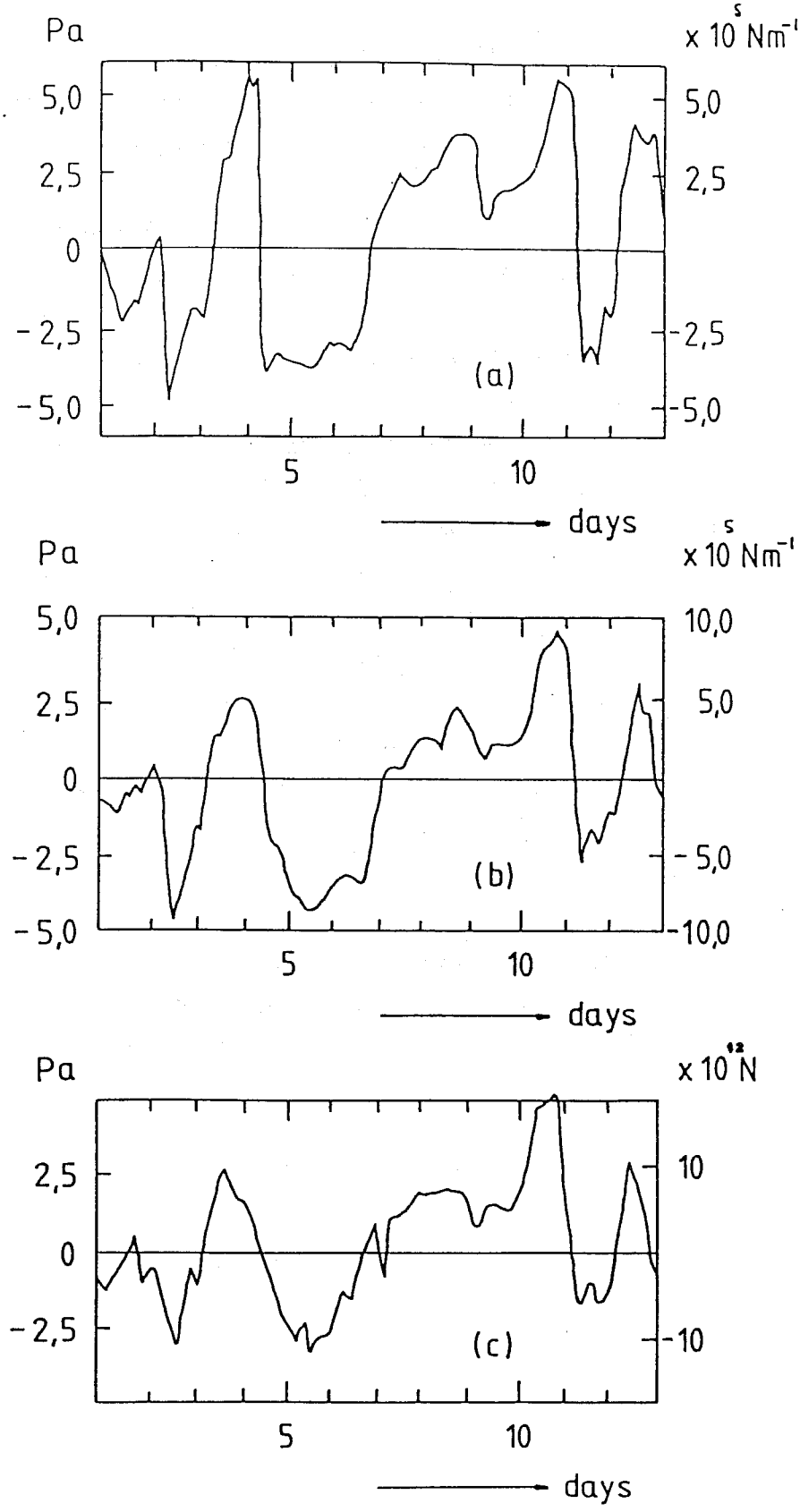

Fig. 3 A semi-schematic depiction of the time-trace of the north-south drag component for the March 1-12 period derived in the studies of (a) DP, (b) H and (c) HS. The right ordinate scale refers in (a,b) to the drag per unit length, and to the drag in (c), whilst the left ordinate scale is a drag per unit area.

Some appreciation of the magnitude of the drag values displayed in Figs. (3a,b) can be gained by reference to the three special cases of momentum balance introduce in section 2.1. To offset a drag per unit area of 5 Pa in the inner-Alpine region would require:

- for case (i), a mean along-ridge compensating velocity of $\gtrsim$ 20 ms^{-1} in the air below the mountain crest ($\sim$ 2.5 km),
- for case (ii), a mean across-ridge potential temperature difference of $\gtrsim$ $4^{o}K$ would be required for the air below crest height,
- for case (iii), such a drag value requires a magnitude for the vertical flux of wave momentum that is almost an order of magnitude larger than most (but not all) observationally inferred values.

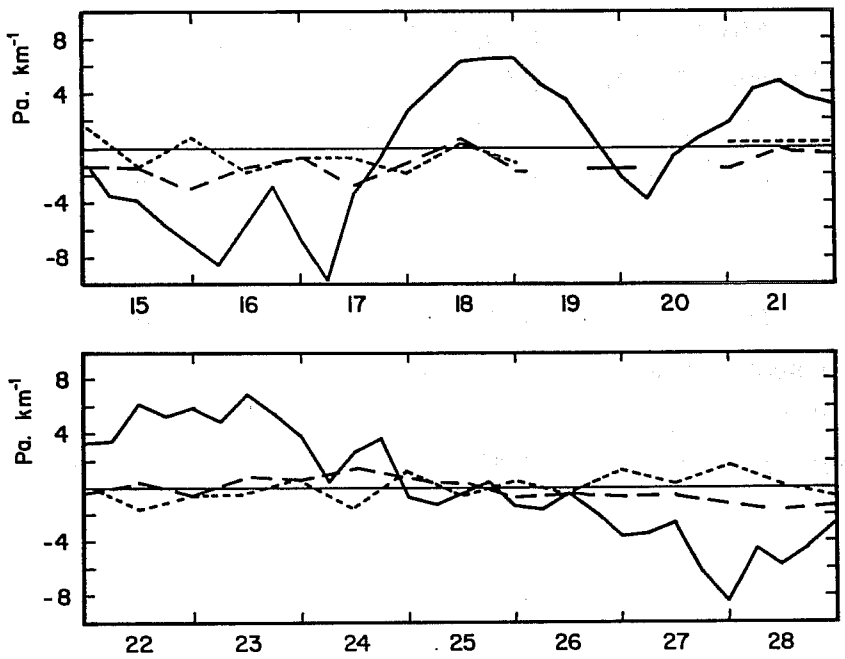

Fig. 4 Time trace for the March 15-28 period of the "surface" horizontal pressure gradient north of the inner Gotthard region (long dashed line), across the Gotthard (solid line) and south of the region (short dashed line).

In the studies of HS and CP estimates were derived for the net (vector) synoptic/sub-synoptic pressure drag acting on the Alps i.e. estimates of $\underset{\sim}{F}$ where $\underset{\sim}{F}$ is (c.f. 2.1) given by,

$$\underset{\sim}{F} = \iint_{S_G} p\,\underset{\sim}{n}\,ds \quad ,$$

or equivalently $= \iiint_V (\nabla_h p)\,dV$.

HS evaluated the drag on four neighbouring segments that together spanned the Alpine massif. They used only a small number of specially selected stations contiguous to the base of the mountain range. The vector $\underset{\sim}{F}$ was estimated subject to the approximation of uniform horizontal pressure gradients in each segment, i.e. $\underset{\sim}{F} \approx (\nabla_h p)V$, and the "artificial" mountain volume was derived using a generalised conical orographic representation in each of the four segments. Shown in Fig. 3c for comparison with the DP and H studies, is the estimate obtained with this method of the north-south component of the drag on the segment spanning the St. Gotthard. The trace is expressed both as the drag (scale on right) and a drag per unit area (scale on left). In CP estimates are presented for east-west and north-south components of the drag for the entire Alps. The drag components were evaluated with a detailed set of surface pressure observations and with various smoothed orographic representations derived from a high resolution data set.

Figs. (5a-d) offer one qualitative comparison of the HS and CP studies. The figures are semi-schematic depictionson a polar diagram of the amplitude and direction of the drag for the two periods of March 4-6 and 9-12. The CP results are those derived with a 0.5^{o} resolution of the orography.

March 4 - 6

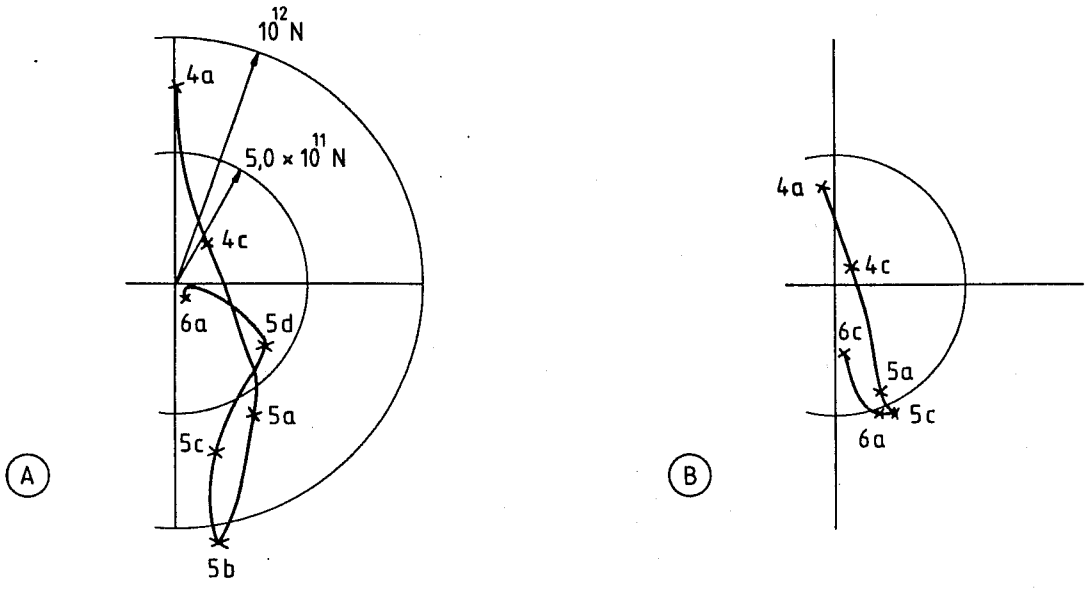

March 9 - 12

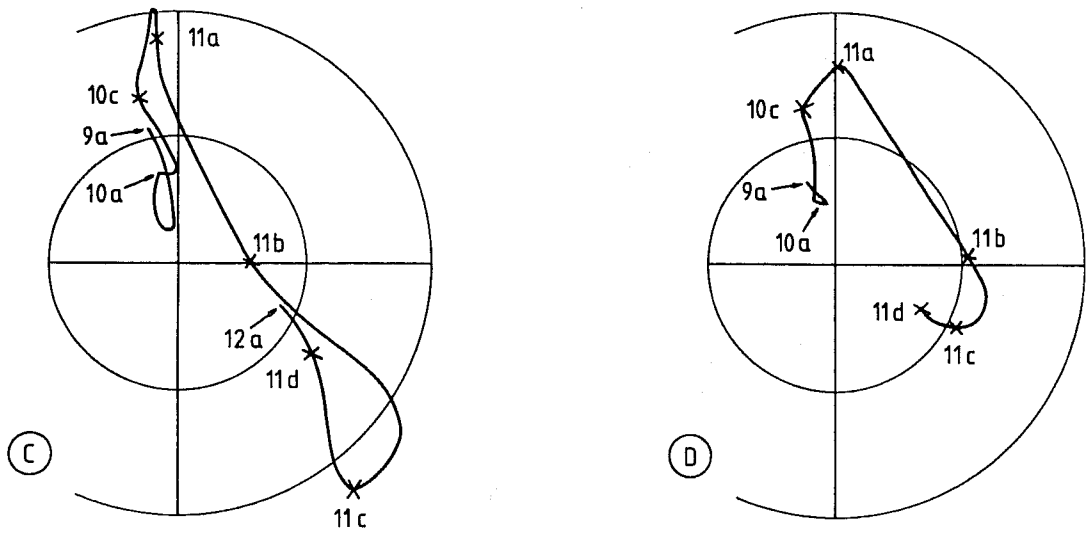

Fig. 5 Semi-schematic polar diagram representations of the amplitude and phase of the "net" pressure drag acting on the entire Alpine massif for the March 3-6 and March 9-12 periods. Plots (A and C) are derived from the results of CP, and plots (B and D) from those of HS. The alpha-numeric notation (e.g. 5c) is such that the numerical refers to the day and (a,b,c,d) signify respectively the times 00Z, 06Z, 12Z, 18Z.

It should be further noted that the horizontal land area over which the drag was estimated was $\sim 40\%$ less in the HS study. In view of this basic difference a direct comparison is not appropriate but it is nevertheless clear that there is a reasonable qualitative correspondence between the results of the two studies. However if the additional land area included in the CP study does not add significantly to (or indeed counteracts) the drag on the Alpine massif itself then the amplitude difference between the results of the studies is indeed physically significant, (c.p. also Fig. 3a, b with Fig.3c). The difference is probably attributable to the coarseness of the orographic profile and the limited number of stations used in the HS study. Indeed CP note a sensitivity of the drag estimates to the resolution of the orographic representation. This sensitivity also indicates that the sub-synoptic/mesoscale orographic features and/or pressure variations are appreciable.

For the results obtained in the HS and CP studies a useful comparative criteria for the amplitude of the net vector drag is the Coriolis lift force ($\sim \rho_0 f U V$) experienced by a mountain range of volume V immersed in an uniform incident flow field (U). For the representation of the Alpine orography considered in HS a value for the pressure force of (5.10^{11} N) would require a value for U of $\sim$ 25 ms^{-1}. Note also that this value of the drag force represents, for the area considered in HS, a drag per unit area of $\sim$ 1.5 Pa compared with typical values of (0.1-0.2) Pa for the drag usually attributed to the momentum stresses assosciated with turbulent panetary boundary layer flow over parkland terrain.

Only a brief overview of these four studies of the drag has been given here. Nevertheless it suffices to indicate that, although the procedural details of the studies make a direct intercomparison of the results difficult, there is a measure of qualitative, and perhaps even quantitative, consistency in the results. Moreover the magnitude of the estimated pressure drag acting on the Alps is appreciable and often exceeds values customarily associated with various conventional drag or lift-inducing mechanisms.

4. INTERPRETATION OF THE DRAG TRACE FOR THE GOTTHARD SECTION

In this section some comments are made on the various signatures associated with the temporal variations of the pressure drag recorded during the ALPEX SOP. The backcloth for our examination is the time trace derived in DP for the drag across the St. Gotthard section of the Alps during the two month March-April 1982 period. This time-trace is shown in Fig.6. Several recurring signatures are identifiable in the trace. Here we adopt a case study approach and consider some of the significant features in relation to the prevailing large scale pressure pattern present during praticular periods.

Type A) Flat synoptic pressure field pattern.

During periods of weak, or quasi-steady, large-scale pressure gradients a diurnal variation is frequently discernible in the drag time-trace. Two examples are the periods of March (24-25) and April (18-19). It was shown in DP that during the SOP this oscillation has a mean amplitude of $\sim 60.10^3$ Nm^{-1} with the maximum and minimum values occuring respectively in early afternoon and after midnight. For the two cited events the drag is established by a $\sim$(1 mb) pressure difference across the orography that extends over a comparatively deep layer ($\sim$1 km), and the ground potential temperature pattern across the St. Gottard ridge shows a tendency for higher values on the southside during the day. Thus thermal forcing due both directly to surface heating and indirectly due to differing "Area-Volume Ratios" (Steinacker, 1984) for the valleys on the north and southside can contribute to the diurnal oscillation. This would suggest that the amplitude of this diurnal effect is a local feature associated with the particular configuration of the orography.

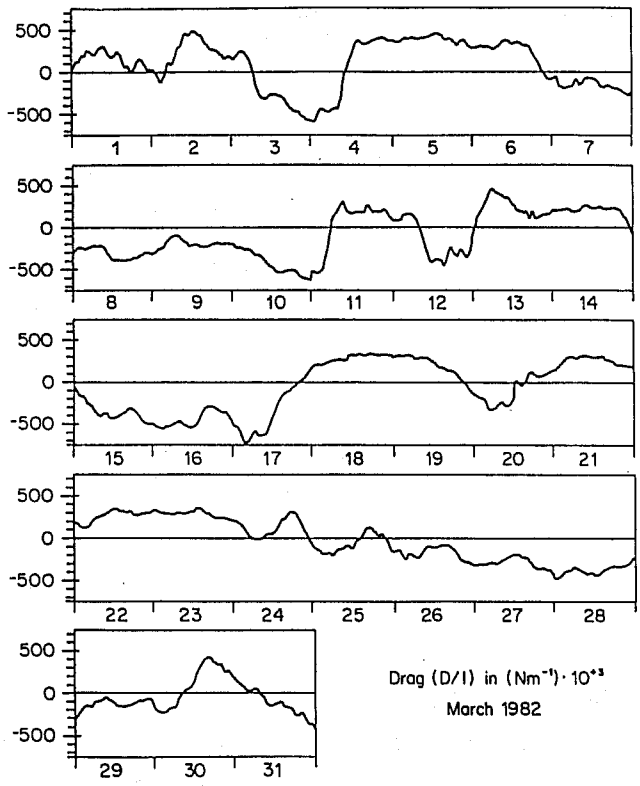

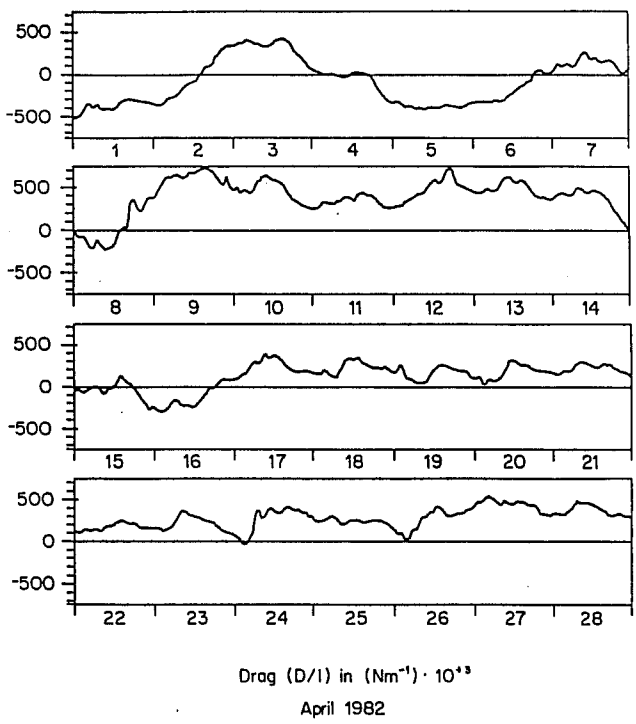

Fig. 6 The estimates derived in DP of the time trace of the pressure drag per unit length for the inner Alpine region of the St. Gotthard. (The conversion to a drag per unit area is 5.10^5 $Nm^{-1} \rightarrow 5$ Pa.)

Type B) An easterly geostrophic flow pattern.

During the March 15-16 period the synoptic scale isobaric and geopotential pattern of the lower troposphere over west-central Europe was aligned essentially east-west. The pattern implied a southward-directed, pressure drag for the St. Gotthard region and easterly geostrophic flow of $\lesssim 5$ ms^{-1} for the air at and below the 700 mb level. In the event the measured drag was small during the first half of March 15, and thereafter appreciable and northward directed with magnitude ($\sim 2.5.10^5$ N m^{-1}) for the subsequent 24 hours, and moreover it was accompanied by a strong (~ 20 ms^{-1}) diurnally varying easterly low-level jet over the northern Alpine foreland. An indication of the structure and variation of this flow along with the accompanying potential temperature pattern can be seen in the spatial latitudinal - height sections shown in Fig. 7. Further details relating to the structure and maintenance of this jet flow are given in Paegle et al (1984) and Wiesel (1986).

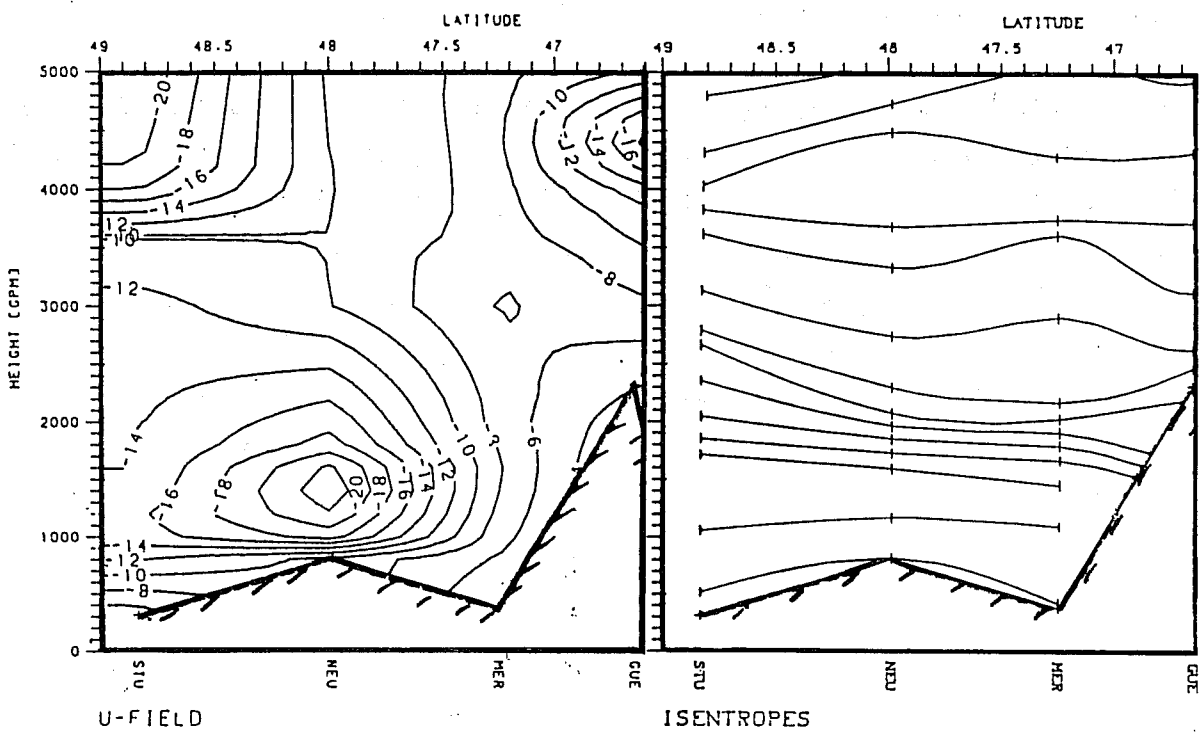

Fig. 7 North-south spatial cross-sections between Stuttgart and Gütsch portraying the isentropic distribution in ^{0}K and west-to-east flow component (in ms^{-1}) at 00Z on April 16, 1982.

A splitting of incident low-level easterly flow would be consistent with theoretical studies (Davies and Horn, 1987) that indicate for a flow tangentially incident upon elongated orography there is a breakdown/ non-existence of steady state semi-geostrophic solutions for flow over isentropic Alpine-scale orography for the typical atmosphere conditions of $R_o \sim 1$ (with R_o based upon the latitudinal half-width of the main ridge). Paegle et al attribute the jet flow and its temporal variation to enhanced flow splitting associated with stable night time conditions. A further intriguing possibility (Horn and Davies, 1986) is that the split low-level flow beneath the inversion exhibits a combined semi-geostrophic and pseudo-hydraulic type response. In this picture the strong night time inversion would generate a sub-critical flow. The resulting pattern is in qualitative agreement with the observations of a mountain trapped band of accelerated easterly flow on the northside of the Alps that is in geostrophic equilibrium with an accompanying latitudinal pressure gradient. This latter gradient is linked to a decrease in the height toward the ridge of the capping inversion.

Type C) A northerly geostrophic flow pattern.

The tropospheric flow to the north of the Alps during the period 27-29 April comprised a deep layer of quasi-steady almost north-south aligned flow. At the surface a succession of weak frontal systems tracked southward over central Europe but for the most part their influence on the region south of Stuttgart was not particularly significant. An indication of the Alpine influence is evident in Fig. 8 which shows the isentropic structure and the southerly and easterly flow components in the 350 km, north-south spatial cross-section between Stuttgart and Milan for 00Z on the 29 April.

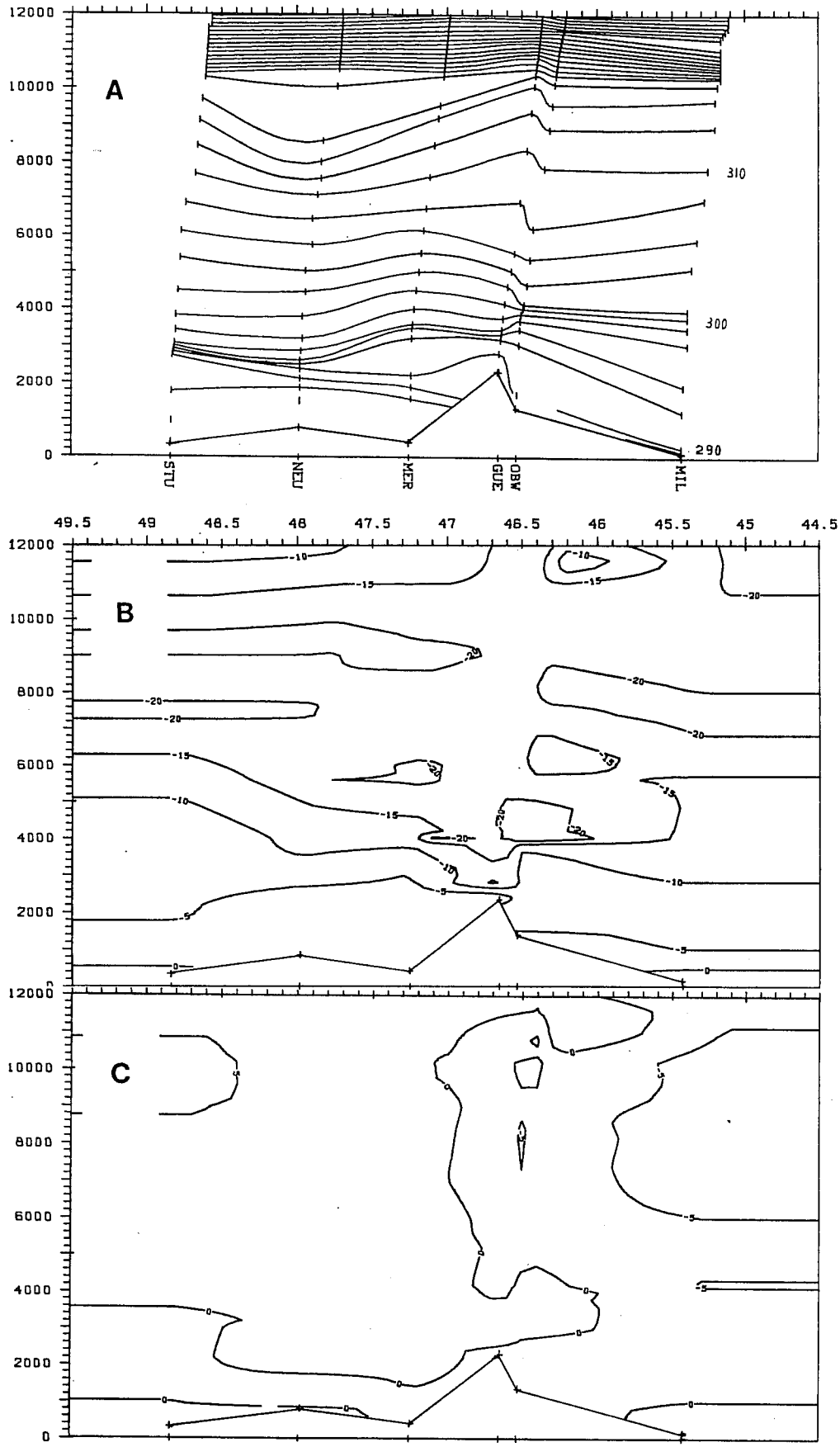

Fig. 8 North-south spatial cross-sections at 00Z 29 April 1982 from Stuttgart to Milan, showing A) the isentropic profils (^{0}K), B) the southerly wind component (ms^{-1}), and C) the easterly wind component (ms^{-1}). Axes refer to latitude and geometric height.

In the upstream region there is an almost purely northerly airstream with a wind maximum $\sim$ 20 ms^{-1} in the 7 - 10 km level, and a strong inversion ($\sim$ $8^{o}K$) at a height of $\sim$ 3 km. The limited data base for this section dictates that caution must be exercised in the interpretation of the flow response. However it is of some interest to note the following features:

- evidence of moderate amplitude mid- and upper-tropospheric wave activity. This feature was not always apparent during this northerly flow episode,
- an isentropic valve above the crest at a height of around 4 km with an accompanying flow speed increase along the stream tube,
- a moderate upstream and downstream acceleration of the flow in the 300-304^{o}K layer,
- an upstream deceleration of the flow below crest height with the suggestion of along-ridge flow variations (i.e. evidence of substantial mass inconsistency between the low level isentropes),
- a weakning/splitting of the inversion particularly downstream of the ridge. This was also a striking feature of the field 24 hours earlier.

These flow features were accompanied by drag values per unit area of $\sim$ 4 Pa (see Fig. 6) linked to a 750 m deep surface layer of appreciable ($\sim$ 3 - 6 mb) cross-Alpine pressure difference. In this case the drag in the north-south section does not appear to be strongly offset by temporal changes or the Coriolis body force. Simple theoretical considerations indicate that the amplitude the drag associated with buoyancy waves should vary with (NU), where U is the incident flow component normal to the ridge. It was shown in DP that this quantity correlated well with the phase of the drag for substantial periods. However independent measurements of the wave-momentum flux aloft (see Hoinka's contribution to this seminar series) suggest that in general the vertical wave transport of momentum offsetsonly a comparatively small percentage of the pressure drag during the ALPEX period. This leaves latitudinal transport of momentum flux as the most probable compensating process for the pressure drag in the momentum budget.

Type D) The frontal signature.

By far the most distinctive recurrent signature in the drag trace is that accompanying the Alpine passage of a frontal system. The episodes of March 1-3, 3-7, 10-12, 12-14, 16-19, 19-21, 30-31 and April 8-9, 23-24 fall into this category.

In the Gotthard signature there are usually two phases . First a period of 1 day with large northward directed drag that preceeds the arrival of a cold front on the immediate Alpine northside followed by a rapid transition to a prolonged period ($\sim$ 1-4 days) of large southward directed drag. This behaviour is also evident in the net vector drag variation on the entire Alps during such events (see Fig. 5 for the examples of the two periods March 3-6 and 9-11). The first prefrontal phase is linked with the occurrence of mild Föhn conditions in the inner Alpine valleys on the northern side along with a significant, but often shallow, southerly wind flow over the main Alpine ridge. The second phase occurs in conjunction with the blocking of the cold air on the Alpine northside and is usually transiently supplemented by the development of a lee cyclone. To the extent that the effects are separable the contribution of the lee cyclone to this second phase might only be secondary compared with that due to the upstream blocking. For example the peak drag values of April 9 (see Fig. 6) were recorded during a minor lee-cyclone event. The second phase, in its fully developed stage, merges with the previous Type C pattern.

Several features associated with this signature are worthy of further attention. Both the time traces (Figs. 3,6) and the polar plots (Fig. 5) establish the prefrontal phase as major drag episode comparable in amplitude and perhaps bearing some underlying physical resemblance to a southerly counterpart of a Type C event.

Also the structure and rapidity of the amplitude and phase changes exhibit a measure of coherency from event to event (see again Figs. 3 and 6). The principal variations from the standard signature take the form of less rapid and/or smaller and less prolonged amplitude changes. Three examples are the events of March 2, 17-18, 20, and these correlate with episodes that exhibit less evidence of upstream blocking.

5. FURTHER REMARKS

The observational studies and interpretations discussed in the previous two sections considered only the sub-synoptic/meso-α scale drag features for the European Alps during the two month period of March-April 1982. It is to be noted that in Spring the Alps are located south of the main track of the mid-latitude cyclones. Also the stronger signatures in the drag pattern, e.g. the frontal signal, appear to be strongly influenced by the major, mesoscale structure of the Alps (main ridge $\sim$ 2.5 km high, 1500 km long, with a lateral half width $\sim$ 75 km). Thus the generality and usefulness of the results are limited by the geographical coverage, the temporal duration and the spatial resolution of the observations.

Nevertheless the large values estimated for the pressure drag are highly significant for the dynamics of the attendant flow. Their amplitude suggests that the orography often sustains pressure forces that are substantially in excess of the Coriolis lift force associated with the prevailing synoptic scale pressure pattern. Indeed on occasions it can be "locally" oppositely directed to the latter force. A frequent effect is the upstream blocking-splitting of the incident airstream which often results in prolonged periods of large pressure drag. A key issue, from the standpoint of numerical weather prediction models, is the contribution of the model "resolvable and unresolvable" flow components to the generation and maintenance of this blocking effect.

REFERENCES

Bell, R.C., and R. Thompson, 1980: Valley ventilation by cross winds. J.Fluid Mech., **96,** 757-767.

Bretherton, F.P., 1969: Momentum transport by gravity waves. Quart.J.Roy.Meteor.Soc., **95,** 213-243.

Carissimo, and R.T. Pierrehumbert, 1986: Mountain drag during ALPEX. (private communication).

Davies, H.C. and J. Horn, 1987: Semi-geostrophic flow of a stratified atmosphere over elongated isentrope valleys and ridges. Tellus (to be published).

Davies, H.C., and P.D. Phillips, 1985: Mountain drag along the Gotthard section during ALPEX. J.Atmos.Sci., **42,** 2093-2109.

Davies, H.C., and C.J. Schär, 1986: Diabatic modification of airflow over a mesoscale orographic ridge: A model study of the coupled response. Quart.J.Roy.Meteor.Soc., **112,** 711-730.

Durran, D.R., 1986: Another look at downslope windstorms. (to be published).

Durran, D.R., and J.B. Klemp, 1983: A compressible model for the simulation of moist mountain waves. Mon.Wea.Rev., **111,** 2341-2361.

Hafner, T.A., 1985: Pressure drag on the European Alps deduced from independent ALPEX data sets. ICAM, Opatija, Zbornik meteoroloskih; hydroloskih radova, **10,** 40-45.

Hafner, T.A., and R.B. Smith, 1985: Pressure drag on the European Alps in relation to synoptic events. J.Atmos.Sci., **42,** 562-575.

Horn, J., 1985: Theoretische Studien und diagnostische Analyse einer stationären Strömung über ein mesoskaliges Gebirge. Diplomarbeit Atmosphärenphysik ETH Zürich, 86 pp.

Horn, J., and H.C. Davies, 1986: Hydraulic theory and observations of a low level jet during ALPEX. ICAM, Rauris. (in press).

Jusem, J.W., and A. Barcilon, 1985: Simulation of moist, mountain waves with an anelstic model. Geophys.Astrophys.Fluid Dynamics, **33,** 259-276.

Klemp, J.B., and D.K. Lilly, 1975: The dynamics of wave-induced downslope winds. J.Atmos.Sci., **32,** 320-339.

Lilly, D.K., and J.B. Klemp, 1979: The effects of terrain shape on nonlinear hydrostatic mountain waves. J.Fluid Mech., **95,** 241-261.

Mason, P.J., 1977: Forces on spheres moving horizontally in a rotating stratified fluid. Geophys.Astrophys. Fluid Dynamics, **8**, 137-154.

Paegle, J., J.N. Paegle, M. McCorcle and E. Miller, 1984: Dignoses and numerical simulation of a low level jet during ALPEX. Beitr. Phys.Atmos., **57**, 419-430.

Peltier, W.R., and T.L. Clark, 1979: The evolution and stability of finite amplitude mountain waves. Part II: Surface wave drag and severe downslope windstorms. J.Atmos.Sci., **36**, 1498-1529.

Pierrehumbert, R.T., 1985: Stratified semi-geostrophic flow over two dimensional topography in an unbounded atmosphere. J.Atmos.Sci., **42**, 523-526.

Pierrehumbert, R.T., and B. Wyman, 1985: Upstream effects of mesoscale mountains. J.Atmos.Sci., **42**, 977-1003.

Steinacker, R., 1984: Area-height distribution of a valley and its relation to the valley wind. Beitr. Phys.Atmos., **57**, 64-71.

Wiesel, E.L., 1986: Synoptic-scale influence on the variability of the ALPEX low-level jet. Proc. Intern. WMO/ICSU Conf. Alpine Experiment Vol.II pp 639-54. WMO Geneva.